



OPEN

Photonic simulation of topological excitations in metamaterials

SUBJECT AREAS:

METAMATERIALS

TOPOLOGICAL INSULATORS

Wei Tan^{1,2*}, Yong Sun^{1*}, Hong Chen¹ & Shun-Qing Shen³

¹Key Laboratory of Advanced Micro-structure Materials, MOE, Department of Physics, Tongji University, Shanghai 200092, China, ²Beijing Computational Science Research Center, Beijing 100084, China, ³Department of Physics, The University of Hong Kong, Pokfulam Road, Hong Kong, China.

Received

6 November 2013

Accepted

6 January 2014

Published

23 January 2014

Correspondence and requests for materials should be addressed to H.C. (hongchen@tongji.edu.cn) or S.-Q.S. (sshens@hku.hk)

* These authors contributed equally to this work.

Condensed matter systems with topological order and metamaterials with left-handed chirality have attracted recently extensive interests in the fields of physics and optics. So far the topological order and chirality of electromagnetic wave are two independent concepts, and there is no work to address their connection. Here we propose to establish the relation between the topological order in condensed matter systems and the chirality in metamaterials, by mapping explicitly Maxwell's equations to the Dirac equation in one dimension. We report an experimental implement of the band inversion in the Dirac equation, which accompanies change of chirality of electromagnetic wave in metamaterials, and the first microwave measurement of topological excitations and topological phases in one dimension. Our finding provides a proof-of-principle example that electromagnetic wave in the metamaterials can be used to simulate the topological order in condensed matter systems and quantum phenomena in relativistic quantum mechanics in a controlled laboratory environment.

The Dirac equation provides a description of relativistic quantum mechanics for an elementary spin-1/2 particle^{1,2}, which predates the discovery of positron, an anti-particle of electron in high energy physics³, and also has extensive applications in condensed matters such as graphene^{4,5} and topological insulators^{6,7}. Recent years it is realized that it is a key to understand topological phases from one to three dimensions and from insulators to superconductors or superfluids⁸. On the other hand, Maxwell's equations form the foundations of classical electrodynamics and modern optics. Modern techniques and material sciences make it possible to precisely control photonic transport in metamaterials, such as negative refraction^{9,10}, electromagnetic cloaking^{11,12}, structure-induced coherence^{13–16}, and mimicking photonic black holes¹⁷. It will be of great interest and importance to link the metamaterials to topological phenomena in condensed matters and the relativistic quantum mechanics. In fact, several proposals have been reported to generate photonic counterparts of quantum Hall edge states^{18–20} and topological insulators²¹ in photonic lattice structures. In these studies, a hexagonal or square lattice was designed to obtain the Dirac point, near which an effective Hamiltonian as well as a Dirac equation was derived in the long wave limit and the topological invariant can be calculated. This demonstrates a link between the topological insulators and electromagnetic media.

Here we demonstrate an alternative approach to simulate topological excitations by mapping explicitly Maxwell's equations to the Dirac equation in one dimension by employing subwavelength metamaterials. The remarkable property of metamaterials lies in their flexibility to have controllable signs and magnitudes of their effective permittivity and permeability. If the permittivity and permeability are simultaneously negative, electromagnetic waves in such metamaterials show left-handed chirality^{9,10}. So far there is no work to address the connection between the topological order and the chirality. We find that the one-dimensional (1D) Maxwell's equations can be written in the compact form which has the identical mathematical structure of the Dirac equation, and consequently perform a proof-of-principle photonic simulation of the Dirac equation in metamaterials by means of the full wave numerical simulation and microwave experiment of transmission line. By tailoring the electromagnetic responses of metamaterials, we successfully implement the band inversion of the Dirac equation. It is noted that the band inversion accompanies change of the chirality of electromagnetic wave in metamaterials from the right-handed to left-handed triad and vice versa, which determines a matter-antimatter correspondence in the relativistic quantum mechanics. For the first time we establish possible relation of the chirality of electromagnetic wave and the topological order. Furthermore we utilize designing metamaterials to observe experimentally the topological phases and excitations in one dimension. This paves the way to investigate the topological phenomena in condensed matters and the Dirac-like particles in high-energy physics in a



photonic simulator²². Meanwhile we can also make use of the solutions of the Dirac equation to understand exotic phenomena observed in metamaterials.

Results

Photonic analog to the Dirac equation. A 1D plane electromagnetic wave of the frequency ω in an optical media can be described by Maxwell's equations

$$-\partial_x E_z = i\omega\mu_0\mu_r(x)H_y, \quad (1)$$

$$\partial_x H_y = -i\omega\epsilon_0\epsilon_r(x)E_z. \quad (2)$$

Here, E_z and H_y are the electric and magnetic fields, ϵ_0 and μ_0 (ϵ_r and μ_r) are the vacuum (dimensionless relative) permittivity and permeability of the media, respectively, which can be functions of position in artificially designed optical materials. By introducing the spinor $\varphi = \begin{pmatrix} \sqrt{\epsilon_0}E_z \\ \sqrt{\mu_0}H_y \end{pmatrix}$, Eqs. (1) and (2) can be written as,

$$[-i\sigma_x\partial_x + m(x)\sigma_z + V(x)]\varphi = E\varphi. \quad (3)$$

Here $m(x) = \frac{\omega}{2c}[\epsilon_r(x) - \mu_r(x)]$ and $V(x) = \frac{\omega}{2c}[\epsilon_r(x) + \mu_r(x) - \langle\epsilon_r(x) + \mu_r(x)\rangle]$ are the effective mass and potential, respectively, $E = -\frac{\omega}{2c}\langle\epsilon_r(x) + \mu_r(x)\rangle$ is the energy eigenvalue, c is the speed of light in vacuum, and $\sigma_{x,y,z}$ are the three Pauli matrices. Equation (3) is equivalent to the stationary Dirac equation in a potential $V(x)$ by taking the Planck constant \hbar and c as units. In this way we have established a one-to-one mapping between Maxwell's equations and the Dirac equation, which provides a platform to study relevant problems of the Dirac equation in metamaterials with engineered permittivity and permeability.

It is noted that the effective mass in Eq. (3) is given by the permittivity and permeability, which can be tailored controllably by artificially designed structures in metamaterials. The signs of permittivity and permeability determine the chirality of electromagnetic wave in optical media: the electric field, magnetic field and the wave vector obey the right-handed or left-handed triad. For ordinary (nonmagnetic) optical materials $\epsilon_r > \mu_r = 1$, the electromagnetic wave obeys the right-handed rule with a positive effective mass $m > 0$ while the double-negative or left-handed metamaterials with $\epsilon_r < \mu_r < 0$ have a negative mass $m < 0$ and obey the left-handed rule. On the other hand, it is known that the sign change of the effective mass accompanying the band inversion is closely related to the topological order of a medium^{23,24}. Therefore, the present study is the first one, to the best of our knowledge, to illustrate the possible relation between topological order in condensed matters and chirality feature in metamaterials. We believe that this relation will open a new route to mimic topological phases and excitations of Dirac equation in designed metamaterials, and to understand some exotic phenomena in metamaterials from a point of view of the Dirac equation.

Simulation of the band inversion in the Dirac equation. The Dirac equation demands the existence of anti-particle, the particles with negative energy and negative mass. The solutions of positive and negative energy automatically satisfy the Einstein mass-energy relation as a consequence of special theory of relativity. To interpret the solutions, Dirac proposed that the negative energy solution is for a positron with negative mass, an anti-particle of electron¹. According to the Pauli exclusion principle, an electron cannot occupy the state of negative energy as all the states with negative energy are supposed to be fully filled. There exists an energy gap $2m_e c^2$ (m_e is the rest mass of electrons) between the positive energy band for an electron and the negative energy band for positron. As the rest mass of electron is very huge, $m_e c^2 = 0.53$ MeV, a positron can only be observed in high energy physics.

However, the mapping between Maxwell's equations and the Dirac equation in 1D offers an alternative approach to realize the band inversion, *i.e.*, the sign change of effective mass in the Dirac equation, because either the permittivity ϵ_r or permeability μ_r in metamaterials can be manipulated in a controllable way²⁵.

Specifically, to bridge the photonic gap and the Dirac gap, we calculate the dispersion relation from the perspective of the Dirac equation as shown in Eq. (3). By treating metamaterials with sub-wavelength unit cell as an effective media with complex electric and magnetic responses, we can obtain the dispersion relation,

$$k^2 = (V - E)^2 - m^2 = \frac{\omega^2}{c^2} \epsilon_r \mu_r. \quad (4)$$

Here k is real if $\epsilon_r \mu_r > 0$, corresponding to either the positive-index band with right-handed chirality or negative-index band with left-handed chirality. In contrast, k has a purely imaginary value if $\epsilon_r \mu_r < 0$, which indicates the existence of a band gap. It follows from Eq. (3) that the gap can be characterized as either positive or negative mass.

Microwave experiments based on transmission-line (TL) metamaterials are performed to realize the band inversion from positive to negative mass. The TLs are all fabricated on copper-clad 1.57-mm thick Rogers RT5880 substrates, whose relative permittivity and tangent loss are $\epsilon_r = 2.2$ and $\tan\delta = 0.0009$, respectively. Two 50- Ω subminiature version A (SMA) connectors are used as the input and output ports. The unit cell of this structure consists of a shunt inductance L in parallel with a capacitance C_0 brought by the TL segment and a capacitance C in series with an inductance L_0 attributed to the TL segment. A circuit model to describe electromagnetic response of the CRLH TL metamaterials was established in Refs. 26 and 27. The validity of the model has been studied extensively in metamaterials, and many novel phenomena based on CRLH TL metamaterials, such as negative refraction and super-resolving lens, are successfully described by the model as summarized in Refs. 28 and 29. It gives the effective permittivity and permeability of the CRLH TL in the long-wavelength limit as,

$$\bar{\epsilon}_r = \frac{1}{p\epsilon_s} \left(C_0 - \frac{1}{\omega^2 L d} \right) + i \frac{\gamma_e}{\omega}, \quad \bar{\mu}_r = \frac{p}{\mu_s} \left(L_0 - \frac{1}{\omega^2 C d} \right) + i \frac{\gamma_m}{\omega}, \quad (5)$$

where ϵ_s and μ_s are the permittivity and permeability of environment media, respectively, C_0 (L_0) is the per-unit-length capacitance (inductance) of the TL segment, C (L) is the series capacitance (the shunt inductance) of the loading elements, γ_e and γ_m denote the losses, d is the length of a unit cell, and p is the geometric factor. We would like to emphasize that these parameters can be tailored experimentally. For example, we can tune the frequency ω or the length of a unit cell d to change the values of the permittivity and permeability continuously. The effective loss in a sample can be deduced from the experimental measurement of transmission and reflection of a sample. It is worthy stressing that the limitation of this model is that the size of each unit cell is required to be smaller than a quarter wavelength. In this experiment, the unit cell has a length of $d = 8$ mm (which is less than 1/10 wavelength in the microstrip), and an electromagnetic wave does not "see" discontinuities of the structure. Thus the CRLH TL can be considered effectively homogenous. From the frequency-dependent ϵ_r and μ_r the two band edges ω_1 and ω_2 are determined by setting $\epsilon_r = 0$ or $\mu_r = 0$, respectively. For simplicity here, we assume $\gamma_e = \gamma_m = 0$, and the band edges is obtained as

$$\omega_1 = \frac{1}{\sqrt{LC_0 d}}, \quad \omega_2 = \frac{1}{\sqrt{L_0 C d}}. \quad (6)$$

The frequency difference between ω_1 and ω_2 defines the energy gap as shown in Fig. 1(a). The gap closing at $\omega_1 = \omega_2$ or $m = 0$ gives rise to the Dirac point, where some interesting behaviors have been reported, such as Zitterbewegung³⁰, wave bending and cloaking



effect³¹. It is clear that the frequencies can be readily tuned by tailoring C_0 , L_0 , C , and L . If we can adjust the band edges from $\omega_1 < \omega_2$ to $\omega_1 > \omega_2$ or vice versa, the band inversion would be achieved.

The band inversion is illustrated in the simulated and measured density of states (DOS) in Fig. 1. Note that both C_0 and L_0 are functions of the width of the TL, w . With an increase of w , C_0 increases, but L_0 decreases. Consequently, one band edge moves to a higher frequency, while the other moves to a lower frequency. Therefore in a well-designed structure, the band inversion is expected to occur by adjusting the width w . We designed several samples and calculated their width-dependent dispersions, and observed the band inversion illustrated in Fig. 1(a). It is noted that the band structure inversion accompanies an exchange of the band edges, and the effective mass also changes its sign. This feature is closely related to the chirality of electromagnetic wave in the designed sample as shown in Fig. 1(b). Before band inversion, the edge of $\mu_r = 0$ locates at higher frequency and connects to the pass band with right-handed chirality for $\epsilon_r > \mu_r > 0$ while the edge of $\epsilon_r = 0$ locates at lower frequency and connects to the pass band with left-handed chirality for $\mu_r < \epsilon_r < 0$, as shown in Fig. 1(b.i). After band inversion from $m > 0$ to $m < 0$, the two band edges are exchanged with each other as shown in Fig. 1(b.iii): the edge of $\mu_r = 0$, for example, moves to the lower frequency and connects to the pass band with left-handed chirality for $\epsilon_r < \mu_r < 0$. The physical picture of the band inversion can be understood as an electromagnetic state (E, H) moving from $(\omega_0 + \Delta\omega, k)$ to $(\omega_0 - \Delta\omega, -k)$ in the dispersion relation, where ω_0 is the frequency of the Dirac point. It is characterized by the sign change of effective mass accompanied by the conversion of electromagnetic chirality. Now it is already known that the sign of the mass in Dirac equation can be used to describe different topological order in condensed matters^{23,24}. Therefore, the above picture shows us a clear connection between topological order in condensed matter systems and chirality in metamaterials: when the chirality of a band changes, its topological order changes.

To illustrate the band structure experimentally we fabricated a series of samples with different widths and measured the DOS for microwaves. Each sample contains 24 units, and each unit has a length of $d = 8$ mm with a series capacitor $C = 3.3$ pF and a shunt inductor $L = 10$ nH. Agilent PNA Network Analyzer N5222A was employed to measure the reflection, transmission, and group delay of the samples. The DOS of a lossless optical system is proportional to the group delay τ_g , $g(\omega) = \frac{1}{\pi} \frac{dk}{d\omega} \propto \frac{\tau_g}{\pi D}$ (where D is the total length of the sample)³². In practice, dissipation is inevitable in the transmission line experiments, and the wave vector k is no longer purely real and the DOS is not well defined. However the group delay is still measurable. When the imaginary part of the effective mass in Eq. (3) is comparably small, it is a good approximation to define the DOS by using the group delay. Meanwhile we also calculated the DOS with a fitted loss from experimental data. The numerical and experimental results are presented in Figs. 1(c) and 1(d), respectively. It is clearly shown that the band gap gradually closes up as w decreases to a critical point of $w_0 = 4.5$ mm. With a further decrease of w , a gap re-opens again. It is worth pointing out that the loss is introduced in the effective permittivity and permeability while the numerical simulation is performed. The values of γ_e and γ_m are taken to be 0.24 by fitting the experimental data. For comparison we also present the result (see the solid line in Fig. 1c) without the loss, the discrepancies between the two cases are very clear. Considering the loss in the sample, the measured data are in a good agreement with the calculated results. In this way we have successfully demonstrated the band inversion in the metamaterials experimentally. This provides an explicit and solid foundation for photonic simulation of the Dirac equation in metamaterials.

Soliton solution for a domain wall. The Jackiw-Rebbi solution describes the bound state of a particle to the interface or domain

wall between two media with positive and negative masses³³. For simplicity consider two 1D media with positive mass $m_1 > 0$ and negative mass $-m_2 < 0$ forming a domain wall at $x = 0$ with a potential $V(x) = 0$. It is found that there exists an analytical solution of zero energy ($E = 0$),

$$\phi(x) = \sqrt{\frac{m_1 m_2}{m_1 + m_2}} \begin{pmatrix} 1 \\ -i \end{pmatrix} \exp[-|m(x)x|], \quad (7)$$

which decays exponentially in $|x|$. It is a solution of 1D topological excitation or soliton, which is robust even for irregular distribution of mass near the interface, and has potential application. For example, the charge carriers in 1D organic conductors are attributed to the solitons and anti-soliton^{34,35}. However, it is still an experimental challenge to observe a single soliton in a 1D polymer due to small lattice spacing^{36,37}. Simulation of the model was also proposed to realize in other systems, such as an atomic Dirac-Fermi gas on an optical lattice³⁸. In metamaterials, a solution for a resonant mode at an interface between two slabs of epsilon-negative and mu-negative media was obtained by solving Maxwell's equations explicitly³⁹ and also confirmed experimentally^{40,41}. However, its topological origin was not recognized so far.

Here we demonstrate that the Jackiw-Rebbi solution can be realized in the metamaterials by constructing a domain wall with controllable parameters. To this end, we fabricated a sample consisting of two TL metamaterials, $w_1 = 2.5$ mm and $w_2 = 8.5$ mm. Both metamaterials have finite gaps, but with opposite masses as illustrated in Figs. 1(c) and 1(d). However, when these two TL metamaterials are connected, it is found that an additional narrow peak appears at $\omega_0 = 11.05$ GHz within the gap region in the DOS as shown in Fig. 2(a). The parameters at $\omega_0 = 11.05$ GHz are given by $m_1 = -11.83$, $V_1 = 0.26 + 0.80i$, $m_2 = 16.65$, and $V_2 = -0.26 + 0.80i$. The corresponding energy of the resonant peak is $E = 0.03$, whose nonzero value is caused by the energy loss or the imaginary part of the potential. Figure 2(b) shows the full-wave simulation of field spatial distribution in the sample at ω_0 , which was obtained by using a commercial software package (CST Microwave Studio). It is clearly seen that the incident field increases to reach a maximal, and then decays exponentially, indicating a well-defined bound state.

We also carried out microwave experiments in time domain to investigate the field distribution. The result is presented in Fig. 2(c), which is in good agreement with the numerical simulation. Note that in each unit cell, only one position near the shunt inductor is probed, and thus the LC resonances within a unit are not detected. The measured peak of the incident field is attributed to the non-linear or topological excitation described by Jackiw-Rebbi solution. Thus this measurement provides the direct observation of the Jackiw-Rebbi solution or the profile of soliton in a photonic simulator made of metamaterials.

Simulation of a 1D lattice topological phase. The metamaterials with different effective masses provide building blocks to construct various artificial optical materials to simulate solid state systems. In condensed matter, the simplest “two-band” model is the Su-Schrieffer-Heeger model for polyacetylene³⁴. Consider a 1D dimerized lattice with bipartite lattice sites A and B. Each unit cell consists of two sites A and B. The hopping amplitude between two sites in a unit cell is $t + \delta t$ and that between two unit cells is $t - \delta t$.

When $\delta t = 0$, the energy dispersion presents $E = \pm 2t \left| \cos \frac{k}{2} \right|$, which exhibits no energy gap at $k = \pi$. However at half filling, due to the Peierls' instability, the dimerization occurs and $\delta t \neq 0$: an energy gap opens, and is equal to $4\delta t$. According to the sign of δt , the gap can be either positive or negative. The inverted band structure is closely related to topological insulators, such as Bi_2Te_3 and Bi_2Se_3 ^{42,43}. The topological property of this 1D model can be also determined by the Berry phase of the lower energy band, which is given by $\pi(\text{sgn}(t +$

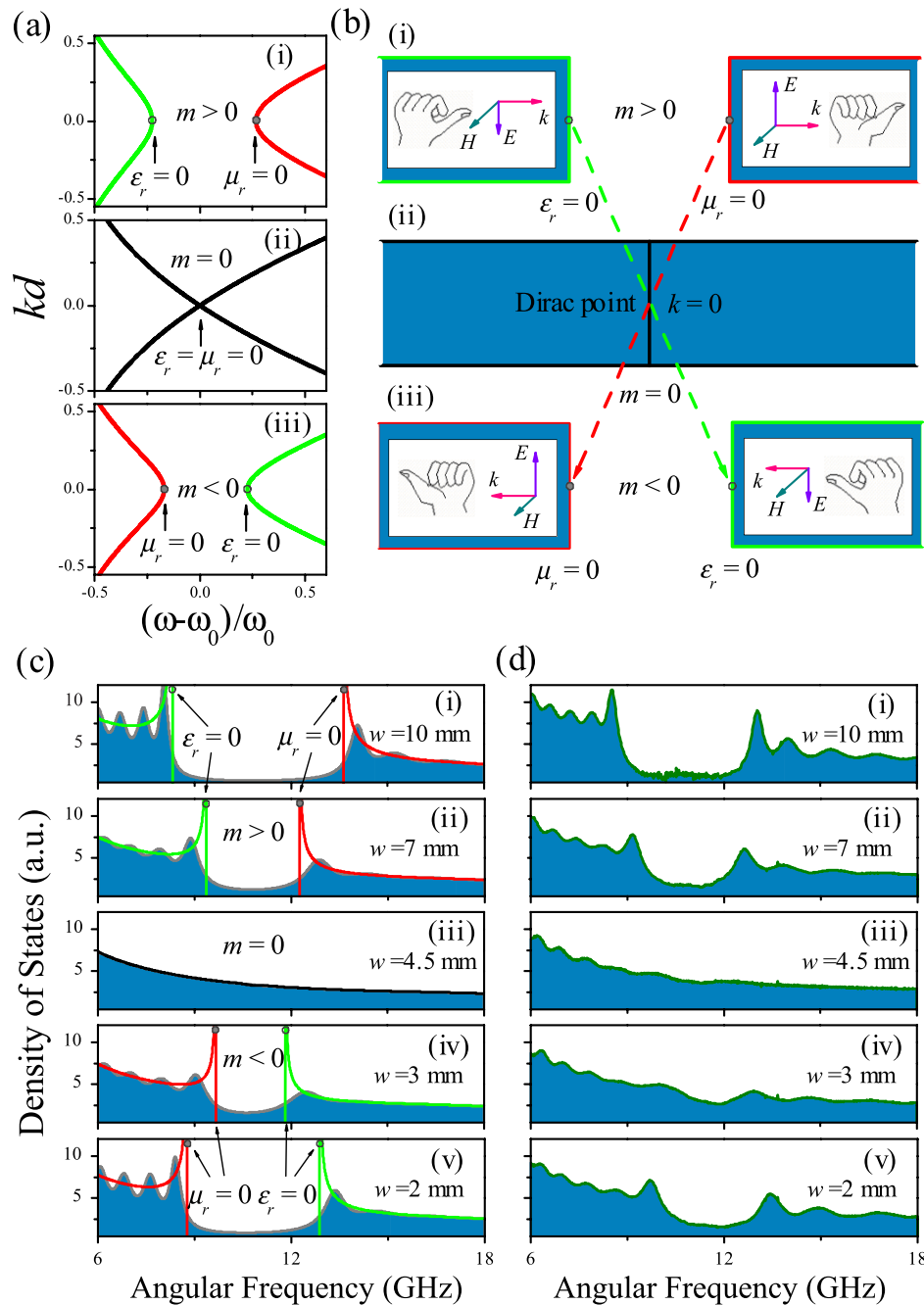


Figure 1 | Photonic simulation of band inversion in the Dirac equation. (a) Calculated dispersion relation for the band structures with (i) $m > 0$, (ii) $m = 0$, and (iii) $m < 0$. $\omega_0 \approx 11.34$ GHz is the frequency when the band gap closes. k is the wave vector and d is the length of a unit cell. (b) The band inversion means the exchange of the band edges and change of chirality from the right-handed triad to the left-handed triad. (c) Calculated density of states for microwave TL samples containing 24 unit cells with fitted losses from experimental data. The solid (red) lines are the DOS spectra for ideal structures without the losses. (d) Measured density of states for microwave TL samples. The losses $\gamma_e = \gamma_m = 0.24$ is adopted in numerical simulation, which is fitted from experimental data.

$\delta t) - \text{sgn}(\delta t)]/2$ modulus by 2π . The difference of the Berry phases for $\delta t > 0$ and $\delta t < 0$ is π , which indicates that the two phases are topologically distinguished: one is topologically trivial and the other one is topological non-trivial. The topologically non-trivial phase is characterized by the presence of end state of zero energy in an open boundary condition^{44,45}. Though it is believed that the end states should exist in 1D polymer, it is a great challenge for experimentalists to measure them experimentally.

To mimic such topological phases in a lattice structure, we design a periodic stack of two TL blocks with $m_A > 0$ ($w = 7$ mm) and $m_B < 0$

($w = 4$ mm), as shown in Figs. 3 and 4(a). The unit of the samples has a length of $d = 7$ mm with a series capacitor $C = 1.0$ pF and a shunt inductor $L = 3.3$ nH, leading to $|m_A| > |m_B|$. This periodic structure can be used to simulate the Su-Schrieffer-Heeger model. Different $m_A > 0$ and $m_B < 0$ corresponds to the positive and negative δt . In the periodic boundary condition, the theoretical calculation shows that dispersion relation have the similar band structure of the Su-Schrieffer-Heeger model, which exhibits the presence of an energy gap $\delta\omega = 1.46$ GHz between two band edges at $\omega_1 = 13.53$ GHz and $\omega_2 = 14.99$ GHz, as shown in Fig. 4(b).

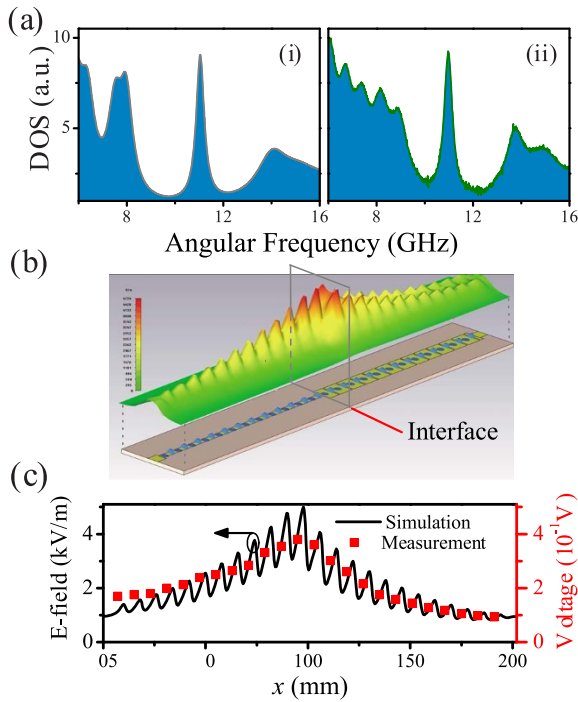


Figure 2 | Domain wall at the interface between two components with opposite masses. (a) Calculated (i) and measured (ii) DOS spectra, exhibiting a bound state within the gap. (b) Full-wave simulation of field distribution of the bound state, presenting localized fields around the interface ($x = 96$ mm). (c) Measured voltage as the field distribution in the sample. The two components are designed with $w_1 = 2.5$ mm and $w_2 = 8.5$ mm, respectively. The parameters at $\omega_0 = 11.05$ GHz are given by $m_1 = -11.83$, $V_1 = 0.26 + 0.80i$, $m_2 = 16.65$, $V_2 = -0.26 + 0.80i$, and $E = 0.03$. For simplicity, we take the losses $\gamma_e = \gamma_m = 0.24$ in numerical simulation, which is fitted from experimental data. It should be noted here that in each unit cell, only one position near the shunt-inductance position is probed.

In the present experiment, we fabricated two structures by removing one block of $m_A > 0$ or $m_B < 0$ from the loop to simulate the 1D polymer in an open boundary condition. The photographs of the two samples are shown in Fig. 3. The measured DOS for microwave

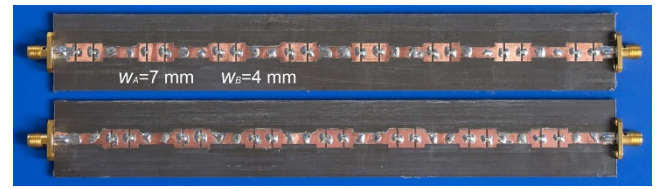


Figure 3 | Fabricated samples for the structures with broken periodic boundary. The two TL blocks have the width of $w_A = 7$ mm and $w_B = 4$ mm, respectively, and have the same length of 14 mm. Each TL block contains two units, and the lumped elements include a series capacitor $C = 1.0$ pF and a shunt inductor $L = 3.3$ nH.

shows that the first case in Fig. 4(c) exhibits a clear gap $\delta\omega = 1.92$ GHz between band edges at $\omega_1 = 13.31$ GHz and $\omega_2 = 15.23$ GHz, whose value is close to the calculated value of the loop. The non-zero DOS is attributed to the loss of the metamaterials, which is characterized by the parameters γ_e and γ_m in Eq. (5). They are fitted to be 0.24 from the measured data. The second case in Fig. 4(d) exhibits a similar band structure as in Fig. 4(c), but presents an additional peak at $\omega_0 = 14.18$ GHz between the two peaks at $\omega_1 = 12.73$ GHz and $\omega_2 = 16.10$ GHz. A more detailed analysis indicates that the two peaks at $\omega_1 = 12.73$ GHz and $\omega_2 = 16.10$ GHz corresponds to the band edges as shown in Fig. 4(b), in which slight shifts of the position are caused by the finite size effect. The resonant peak at $\omega_0 = 14.18$ GHz corresponds to two bound states at the ends, which can be seen clearly in Figs. 4(e) and 4(f). This indicates that the topological properties of the two designed chains are topologically distinguished, although they are constructed by the same blocks of $w = 7$ mm and $w = 4$ mm. Thus our measurements demonstrate explicitly the existence of the end states in 1D topological systems.

Discussion

In summary, we have demonstrated an explicit mapping between Maxwell's equations and the Dirac equation in one dimension. This provides a platform to utilize the electromagnetic wave to mimic quantum phenomena related to the Dirac equation from high-energy physics to condensed matter physics. In the form of the Dirac equation, the effective mass is determined by the permittivity and permeability of the media. While the absolute sign of mass has no special physical meaning, the sign change of the mass is closely related to the topological order of a medium. We can make use of this property to

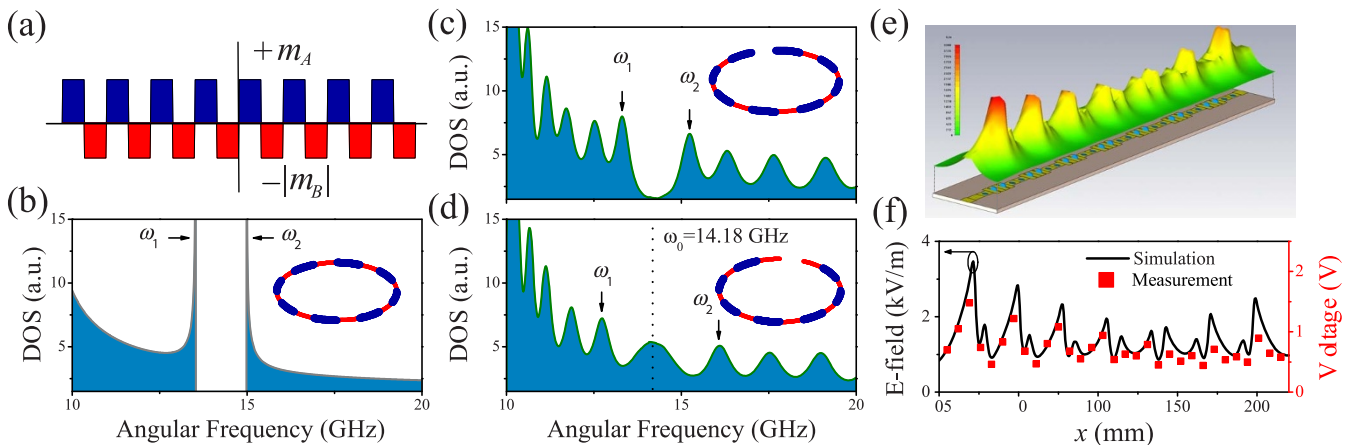


Figure 4 | Topological properties of a lattice structure. (a) Scheme of the periodic structure composed of the components of $m_A > 0$ and $m_B < 0$. (b) DOS of the ideal periodic structure. A band gap of $\delta\omega = 1.46$ GHz is present between $\omega_1 = 13.53$ GHz and $\omega_2 = 14.99$ GHz. (c) The measured DOS for the structure with an open boundary condition by removing one block of $m_A > 0$ component. Two band edges appear at $\omega_1 = 13.31$ GHz and $\omega_2 = 15.23$ GHz. (d) The measured DOS for the structure lacking of a $m_B < 0$ component. Two band edges appear at $\omega_1 = 12.73$ GHz and $\omega_2 = 16.10$ GHz, and a resonant peak for the end mode appears at $\omega_0 = 14.18$ GHz. Inset, schemes of the structures in three cases. (e) Full-wave simulation of field distribution of the end mode corresponding to (d). (f) Measured voltage as the field distribution in the sample.



generate photonic counterparts of 1D topological excitations. By tailoring the permittivity and permeability of metamaterials, band inversion of the Dirac equation was demonstrated theoretically and experimentally. It has been found that the band inversion accompanies a change of chirality of electromagnetic wave in metamaterials. Furthermore, we have designed and fabricated transmission-line structures to demonstrate some important solutions of the Dirac equation, such as soliton solution for a domain wall and the Su-Schrieffer-Heeger model for polyacetylene. Different from the previous topological excitations in two-dimensional photonic lattice structures where an effective Dirac equation was derived near the Dirac point in a long wave limit^{18–21}, we write the 1D Maxwell's equations explicitly in the form of Dirac equation and propose to stimulate topological excitations by engineering the electromagnetic responses of metamaterials. Our numerical simulation and microwave experiments illustrated a proof-of-principle example that metamaterials are ideal candidates to simulate topological phenomena in solids, and the behaviors of the Dirac equation.

Methods

The TLs are all fabricated on copper-clad 1.57-mm thick Rogers RT5880 substrates. A network analyzer (Agilent PNA N5222A) was used to characterize our samples in frequency domain. Transmission and reflection properties were obtained directly, and the density of states is calculated from the measured group delay. Then we carried out microwave experiments in time domain to investigate the field distribution. At the particular frequency, a monochromatic wave generated from Agilent E8267D is input to the sample. After that, voltage signals at the different positions along the sample are picked and recorded, using the high-impedance active probe (Tektronix P7260) and the oscilloscope (Tektronix TDS7704B). In each unit cell, only one position which is near the shunt inductor is probed, and thus the LC resonances within a unit are not detected.

Numerical simulations were obtained using a commercial software package (CST Microwave Studio). Full methods, specific parameters of the samples, and experiment measurement are available in the Supplementary Informations.

1. Dirac, P. A. M. The quantum theory of the electron. *Proc. R. Soc. A* **117**, 610–624 (1928).
2. Dirac, P. A. M. *Principles of quantum mechanics*, 4th edition (Clarendon, 1982).
3. Anderson, C. D. The positive electron. *Phys. Rev.* **43**, 491–494 (1933).
4. Novoselov, K. S. *et al.* Two-dimensional gas of massless Dirac fermions in graphene. *Nature* **438**, 197–200 (2005).
5. Zhang, Y., Tan, J. W., Stormer, H. L. & Kim, P. Experimental observation of the quantum Hall effect and Berry's phase in graphene. *Nature* **438**, 201–204 (2005).
6. Hasan, M. Z. & Kane, C. L. Topological insulators. *Rev. Mod. Phys.* **82**, 3045–3067 (2010).
7. Qi, X. L. & Zhang, S. C. Topological insulators and superconductors. *Rev. Mod. Phys.* **83**, 1057–1110 (2011).
8. Shen, S. Q. *Topological insulators* (Springer-Verlag, Berlin, 2012).
9. Pendry, J. B. Negative refraction makes a perfect lens. *Phys. Rev. Lett.* **85**, 3966–3969 (2000).
10. Shelby, R. A., Smith, D. R. & Schultz, S. Experimental verification of a negative index of refraction. *Science* **292**, 77–79 (2001).
11. Leonhardt, U. Optical conformal mapping. *Science* **312**, 1777–1780 (2006).
12. Pendry, J. B., Schurig, D. & Smith, D. R. Controlling electromagnetic fields. *Science* **312**, 1780–1782 (2006).
13. Papasimakis, N., Fedotov, V. A., Zheludev, N. I. & Prosvirnin, S. L. Metamaterial analog of electromagnetically induced transparency. *Phys. Rev. Lett.* **101**, 253903 (2008).
14. Zheludev, N. I., Prosvirnin, S. L., Papasimakis, N. & Fedotov, V. A. Lasing spaser. *Nat. Phot.* **2**, 351–354 (2008).
15. Liu, N. *et al.* Plasmonic analogue of electromagnetically induced transparency at the Drude damping limit. *Nat. Mater.* **8**, 758–762 (2009).
16. Luk'yanchuk, B. *et al.* The Fano resonance in plasmonic nanostructures and metamaterials. *Nat. Mater.* **9**, 707–715 (2010).
17. Genov, D. A., Zhang, S. & Zhang, X. Mimicking celestial mechanics in metamaterials. *Nat. Phys.* **5**, 687–692 (2009).
18. Haldane, F. D. M. & Raghu, S. Possible Realization of Directional Optical Waveguides in Photonic Crystals with Broken Time-Reversal Symmetry. *Phys. Rev. Lett.* **100**, 013904 (2008).
19. Wang, Z., Chong, Y., Joannopoulos, J. D. & Soljacic, M. Observation of unidirectional backscattering-immune topological electromagnetic states. *Nature* **461**, 772 (2009).
20. Hafezi, M., Demler, E. A., Lukin, N. D. & Taylor, J. M. Robust optical delay lines with topological protection. *Nat. Phys.* **7**, 907 (2011).

21. Khanikaev, A. B. *et al.* Photonic topological insulator. *Nat. Mater.* **12**, 233 (2013).
22. Aspuru-Guzik, A. & Walther, P. Photonic quantum simulators. *Nat. Phys.* **8**, 285–291 (2012).
23. Bernevig, B. A., Hughes, T. L. & Zhang, S. C. Quantum spin Hall effect and topological phase transition in HeTe quantum wells. *Science* **314**, 1757–1761 (2006).
24. Lu, H. Z., Shan, W. Y., Yao, W., Niu, Q. & Shen, S. Q. Massive Dirac fermions and spin physics in an ultrathin film of topological insulator. *Phys. Rev. B* **81**, 115407 (2010).
25. Jiang, H. *et al.* Properties of one-dimensional photonic crystals containing single-negative materials. *Phys. Rev. E* **69**, 066607 (2004).
26. Caloz, C. & Itoh, T. Application of the transmission-line theory of left-handed (LH) materials to the realization of a microstrip 'LH line'. *IEEE AP-S International Antenna and Propagation Symposium Digest* **2**, 412–415 (2002).
27. Iyer, A. K. & Eleftheriades, G. V. Negative refractive index metamaterials supporting 2-d wave. *IEEE MTT-S International Microwave Symposium Digest* **2**, 1067–1070 (2002).
28. Iyer, A. K. & Eleftheriades, G. V. Negative-refractive-index transmission-line metamaterials. *Negative-Refractive Metamaterials: Fundamental Principles and Applications*, Eleftheriades, G. V. & Balmain, K. G. (ed.) [1–52] (John Wiley & Sons, Inc., New Jersey, 2005).
29. Caloz, C. & Itoh, T. *Electromagnetic Metamaterials: Transmission Line Theory and Microwave Applications* (Wiley, New York, 2006).
30. Zhang, X. Observing Zitterbewegung for photons near the Dirac point of a two-dimensional photonic crystal. *Phys. Rev. Lett.* **100**, 113903 (2008).
31. Huang, X., Lai, Y., Hang, Z. H., Zheng, H. & Chan, C. T. Dirac cones induced by accidental degeneracy in photonic crystals and zero-refractive-index material. *Nat. Mater.* **10**, 582–586 (2011).
32. Bendickson, J. M., Dowling, J. P. & Scalora, M. Analytic expressions for the electromagnetic mode density in finite, one-dimensional, photonic band-gap structures. *Phys. Rev. E* **53**, 4107 (1996).
33. Jackiw, R. & Rebbi, C. Solitons with fermion number $\frac{1}{2}$. *Phys. Rev. D* **13**, 3398–3409 (1976).
34. Su, W. P., Schrieffer, J. R. & Heeger, A. J. Solitons in polyacetylene. *Phys. Rev. Lett.* **42**, 1698–1701 (1979).
35. Heeger, A. J., Kivelson, A. J., Schrieffer, J. R. & Su, W. P. Solitons in conducting polymers. *Rev. Mod. Phys.* **60**, 781–850 (1988).
36. Brazovskii, S., Brun, C., Wang, Z. Z. & Monceau, P. Scanning-tunneling microscope imaging of single-electron solitons in a material with incommensurate charge-density waves. *Phys. Rev. Lett.* **108**, 096801 (2012).
37. Zhang, H. *et al.* Atomic structure, energetics, and dynamics of topological solitons in indium chains on Si(111) surfaces. *Phys. Rev. Lett.* **106**, 026801 (2011).
38. Ruostekoski, J., Dunne, G. V. & Javanainen, J. Particle number fractionalization of an atomic Fer-Dirac gas in an optical lattice. *Phys. Rev. Lett.* **88**, 180401 (2002).
39. Alu, A. & Engketa, N. Pairing an epsilon-negative slab with a mu-negative slab: resonance, tunneling and transparency. *IEEE Trans. Antenna Propag.* **51**, 2558 (2003).
40. Fujishige, T., Caloz, C. & Itoh, T. Experimental demonstration of transparency in ENG-MNG pair in a CRLH transmission-line implementation. *Microwave Opt. Technol. Lett.* **46**, 476 (2005).
41. Feng, T. H. *et al.* Highly localized mode in a pair structure made of epsilon-negative and mu-negative metamaterials. *J. Appl. Phys.* **104**, 013107 (2008).
42. Zhang, H. J. *et al.* Topological insulators in Bi₂Se₃, Bi₂Te₃ and Sb₂Te₃ with a single Dirac cone on the surface. *Nat. Phys.* **5**, 438–442 (2009).
43. Xia, Y. *et al.* Observation of a large-gap topological insulator class with a single Dirac cone on the surface. *Nat. Phys.* **5**, 398–402 (2009).
44. Ryu, S. & Hatsugai, Y. Entanglement entropy and the Berry phase in the solid state. *Phys. Rev. B* **73**, 245115 (2006).
45. Shen, S. Q., Shan, W. Y. & Lu, H. Z. Topological insulator and the Dirac equation. *Spin* **1**, 33–44 (2011).

Acknowledgments

We acknowledge discussions with Liang Chen. The work was supported by National Basic Research Program (973) of China under Grant No.: 2011CB922001 (HC), Nature Science Foundation of China under Grant Nos.: 11234010 (HC) and 11204217 (YS), and Research Grant Council of Hong Kong under Grant No.: N_HKU748/10 (SQS).

Author contributions

H.C. and S.Q.S. conceived and designed the experiments. Y.S. carried out the sample fabrication and the measurements. W.T. carried out the numerical simulation. S.Q.S. and W.T. provided theoretical analysis and interpretation. All authors co-wrote the paper.

Additional information

Supplementary information accompanies this paper at <http://www.nature.com/scientificreports>

Competing financial interests: The authors declare no competing financial interests.



How to cite this article: Tan, W., Sun, Y., Chen, H. & Shen, S.-Q. Photonic simulation of topological excitations in metamaterials. *Sci. Rep.* 4, 3842; DOI:10.1038/srep03842 (2014).



This work is licensed under a Creative Commons Attribution-NonCommercial-NoDerivs 3.0 Unported license. To view a copy of this license, visit <http://creativecommons.org/licenses/by-nc-nd/3.0>